Int. J. Heat Mass Transfer. Vol. 33, No. 9, pp. 1795–1803, 1990
Printed in Great Britain

0017-9310/90 $3.00 + 0.00
Pergamon Press plc

Mechanisms and predictions of burnout in flow boiling over heated surfaces with an impinging jet

M. KANDULA
Lockheed Engineering and Sciences Company, Houston, TX 77258, U.S.A.

(*Received* 16 *May* 1989 *and in final form* 15 *September* 1989)

Abstract—A physical model is proposed for the mechanism of boiling burnout in saturated forced convection on heated discs cooled by liquid jets impinging normal to the surface. It is postulated that the relative velocity between the liquid and vapor bubbles in the film governs the burnout process. Two distinct critical heat flux (CHF) regions have been recognized. When the liquid and vapor velocities are of the same order of magnitude, typical of low pressures, burnout results from droplet splash and is surface tension-controlled. At low vapor velocities relative to the liquid, typical of high pressures, burnout appears to result from the separation of the liquid boundary layer, and is controlled by liquid viscosity. Correlation of the model predictions for CHF with the available data for a wide range of liquid–vapor density ratios has provided new insight into the scaling and the splashing rate of droplets. A criterion for transition between the two CHF regimes is also suggested.

1. INTRODUCTION

RECENT STUDIES on flow boiling have shown that very high critical heat fluxes (CHF) are achieved when impinging liquid jets are used to cool heated surfaces [1–6]. For instance, with a 2 mm diameter saturated water jet at 1 atm, CHF of up to 10 MW m^{-2} can be achieved [7], which is ten times the corresponding value for pool boiling. Much higher heat fluxes can be realized at increased system pressures and with initial subcooling of the jet. Thus, there seems to be a great potential for boiling liquid jets in meeting some modern demands of technology.

Accurate representation of the physical processes of burnout is central to the prediction of peak heat flux in such systems. Although considerable knowledge was gained regarding the burnout phenomenon in pool boiling, there is limited information on burnout processes in flow boiling with impinging jets.

Boiling characteristics of the impinging liquid jets were first clarified by the excellent observations of Katto *et al.* [1–5] using water, R-113 and R-12 over a wide range of system pressures. The radial flow of the thin liquid film from the stagnation point is accompanied by bubble burst and droplet splashing. Uncertainties regarding droplet size and the rate of droplet splash from the film complicates the prediction of CHF.

As a result, the proposed correlations for CHF are primarily empirical or semi-empirical. Katto *et al.* [1–6] presented correlations based on dimensional analysis. Lienhard *et al.* [7–9] reported a continuous correlation using the mechanical energy stability criterion [7], in conjunction with the data of Katto *et al.* [1–4]. Although these correlations predict CHF with reasonable accuracy over a wide range of conditions, they do not present a unified theory of the burnout processes.

In this paper, a physical model is proposed for burnout mechanisms for impinging jets. The critical heat flux data of Katto and Shimizu [3] are recorrelated in a more general form based on the proposed mechanisms. A correlation for the droplet splash rate as a function of the liquid–vapor density ratio is generated from the modified form of the CHF correlation in the low velocity region. It is further shown that the transition Weber number between the low and high velocity regions depends on the density ratio of the fluid and an additional dimensionless group involving the ratio of liquid viscosity and surface tension.

2. FLOW STRUCTURE

Figure 1 shows the jet–disc configuration to be analyzed. The impinging jet forms a spreading sheet in the radial direction. Various flow regimes have been noticed in the absence of boiling for an upward facing surface.

Homann [10] studied the stagnation zone, $r' = O(d/2)$, when the freestream velocity rises rapidly from 0 to $r' = 0$ to the jet velocity u_j according to

$$u_{f,\infty} = ar' \tag{1a}$$

where a is the stagnation velocity gradient. Laminar boundary layer thickness, δ', in this region is constant and of $O(\nu_f d/2u_j)^{1/2}$, since the thinning due to freestream acceleration exactly balances the thickening due to shear diffusion [11, 12].

A detailed boundary layer treatment of the liquid film away from the stagnation zone was provided by Watson [13]. For $r' \gg d/2$, a Blasius-type boundary layer with a constant freestream velocity $u_{f,\infty} = u_j$ was considered up to $r' = D_0/2$, where D_0 is given by

$$D_0/d = 0.3667 Re_j^{1/3}. \tag{1b}$$

NOMENCLATURE

a	constant
C_1, C_2, C_3	constants
C_f	skin-friction coefficient
d	jet diameter
D	disc diameter
E	rate of energy
g_c	Newton constant
G	mass flow rate of jet
G_d	mass flow rate of splashed droplets
h_{fg}	latent heat of vaporization
$\dot{m}$	mass flow rate
M	molecular weight
n	nucleation site density per unit area
p	system pressure
q_{max}	peak, critical or burnout boiling heat flux
q_w	wall heat flux in nucleate boiling
r'	radial location
r	ρ_f/ρ_g
R	universal gas constant
Re_j	jet Reynolds number, $\rho_f u_j d/\mu_f$
t	residual film thickness
t_0	film thickness in the absence of splashing
T_c	critical temperature (absolute)
T_{sat}	saturation temperature
T_w	wall temperature
ΔT	wall superheat, $T_w - T_{sat}$
u_f	radial velocity in the liquid film
u_g	vapor velocity (superficial) normal to the wall (y-direction)
u_j	jet velocity
We_f	liquid Weber number, $\rho_f u_j^2 D/\sigma$.

Greek symbols

α	fraction of liquid flow directed into spray, G_d/G
β	D/d
γ	defined by equation (29b)
δ	characteristic droplet diameter
δ'	boundary layer thickness
η	$\sqrt{(\omega g_c R T_c/M)}$
μ_f	liquid viscosity
ν_f	liquid kinematic viscosity
ρ_f, ρ_g	saturated liquid and vapor densities
σ	surface tension
ϕ	$u_{g,max}/u_j = q_{max}/(\rho_g h_{fg} u_j)$
ω	Pitzer's acentric factor.

Subscripts

c	critical state
d	droplet
f	liquid film
g	vapor
j	jet
∞	freestream.

Superscript

$\bar{}$	average.

The boundary layer thickness in this region is $O(\nu_f r'/2u_j)^{1/2}$, and becomes comparable to the film thickness $t_0 = O(d^2/r')$ where $r' = O((d/2)Re_j^{1/3})$. At $r' = D_0/2$, the boundary layer thickness is equal to the film thickness.

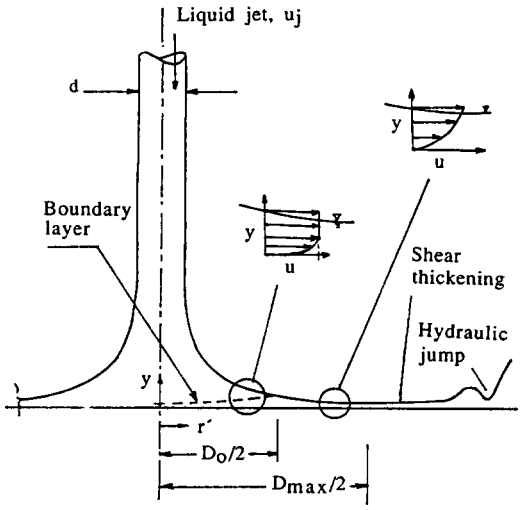

FIG. 1. A schematic of the jet–disc configuration.

For $r' > D_0/2$, a parabolic similarity profile was considered with a decelerating freestream ($du_{f,\infty}/dr' < 0$). It has been shown that the sheet thickness has a minimum at $r' = D_{max}/2$, where D_{max} is given by

$$\beta_{max} = D_{max}/d = 0.5245 Re_j^{1/3} \tag{1c}$$

with the minimum thickness $t_{0,min}$ expressed as

$$t_{0,min} \approx 0.22 \frac{d}{2} Re_j^{1/3}. \tag{1d}$$

Viscosity was thus shown to slow the sheet, so the liquid film thins out less rapidly. In fact, the film starts to thicken as the freestream velocity diminishes far enough. At some position, probably for $r' > D_{max}/2$, a hydraulic jump may be initiated which can be located by equating the rate of loss of momentum to the hydrostatic pressure thrust.

The presence of boiling can alter the above flow structure, as will be discussed in the following sections.

3. PHYSICAL MODEL FOR BURNOUT

Possible mechanisms of burnout in the jet–disc configuration are illustrated in Fig. 2. It is postulated that

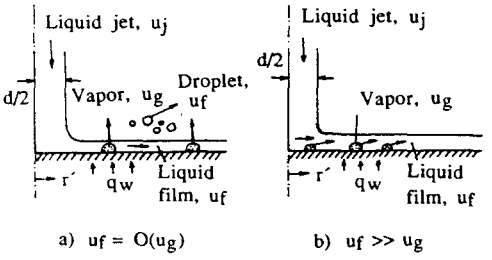

FIG. 2. Proposed mechanisms of burnout in jet–disc configuration.

the relative velocity between the radially flowing liquid film and the vertically moving vapor due to bubble generation at the surface plays an essential role in the burnout process. Two distinct boiling regimes could then be identified.

Region 1 is depicted in Fig. 2(a), where the liquid velocity in the film is of the same order of magnitude as the vapor velocity, i.e. $u_f = O(u_g)$. It is presumed that droplets with a size distribution are generated by bubbles bursting through the flowing liquid film. As a result, the droplets may move at an average velocity u_d at some angle to the surface such that they probably do not redeposit on the film. The droplet formation is linked to surface tension and inertia forces, and so the burnout in this situation should be controlled by surface tension. Region 1 is, therefore, termed as the surface tension-controlled regime or σ-regime.

Figure 2(b) describes region 2, where the film velocity is far in excess of the vapor velocity $u_f \gg u_g$. The bubbles generated at the surface will not have enough momentum to escape from the film, but are dragged along radially by the film inertia. Thus, the probability of droplet generation in this mode is relatively small. It is speculated that burnout under these conditions could result from the separation of the liquid boundary layer due to vapor blowing and blanketing, and is controlled by liquid viscosity. Region 2 is thus termed the liquid viscosity-controlled regime or μ-regime.

4. PREDICTION OF CHF

Separate analyses are made to predict the CHF in the σ- and μ-regions for describing the different mechanisms at burnout as postulated.

4.1. *Surface tension-controlled regime (or σ-region)*

The following assumptions are made in analyzing CHF in the σ-region.

(1) The flow past the heated surface is potential, due to destruction of the boundary layer by the vapor generation at the surface and subsequent tearing of the liquid film.

(2) Flow is nearly radial, with a constant freestream velocity $u_f = u_j$. This assumption is justified for $r' > a$.

With the above assumptions, we now apply the mechanical energy stability criterion as originally reported in ref. [7] for the jet–disc system. It states that at burnout the rate of mechanical energy supplied to the wake configuration equals that absorbed by it.

Rate of kinetic energy of jet + Rate of kinetic energy of vapor = Rate of surface energy of droplets + Rate of kinetic energy of liquid (film + droplets). (2)

This can be expressed as

$$u_f\left(\frac{\pi}{4}d^2\right)\frac{\rho_f u_f^2}{2} + u_g\left(\frac{\pi}{4}D^2\right)\frac{\rho_g u_g^2}{2} = \alpha_c \frac{\rho_f u_f (\pi/4)d^2}{\rho_f(\pi/6)\delta^3}\pi\delta^2\sigma + \left\{(1-\alpha_c)\rho_f u_f\left(\frac{\pi}{4}d^2\right)\frac{u_f^2}{2} + \alpha_c\rho_f u_f\left(\frac{\pi}{4}d^2\right)\frac{u_d^2}{2}\right\}. \quad (3)$$

In the above relation, δ is the characteristic drop diameter, and α is the fraction of the liquid splashed as droplets defined by

$$\alpha = \frac{\dot{m}_d}{\dot{m}} \quad (4)$$

where

$$\dot{m} = \dot{m}_f + \dot{m}_d + \dot{m}_g = \frac{\pi}{4}d^2\rho_f u_f. \quad (5)$$

Assuming that the droplets keep their original momentum, the drop velocity is taken close to u_f, i.e. $u_f = u_d$. Then the kinetic energy of the vapor generated balances the surface energy of the droplets. That is

$$u_g\left(\frac{\pi}{4}D^2\right)\frac{\rho_g u_g^2}{2} = \alpha_c \frac{\rho_f u_f(\pi/4)d^2}{\rho_f(\pi/6)\delta^3}\pi\delta^2\sigma \quad (6)$$

where δ is an average characteristic droplet diameter.

In terms of the dimensionless critical heat flux defined by

$$\phi = \frac{q_c}{\rho_g h_{fg} u_j} \cong \frac{u_g}{u_j} \quad (7)$$

equation (6) can be expressed as

$$\phi \sim \alpha_c^{1/3}\left(\frac{d}{\delta}\right)^{1/3}\frac{r^{1/3}}{(\beta\, We_f)^{1/3}}. \quad (8)$$

Great uncertainties presently exist on the estimation of the droplet diameter δ and the rate of droplet splash α_c.

4.1.1. *Droplet diameter.* The mechanism of droplet formation in this case is basically different from that usually observed in spray nozzles or annular gas–liquid flows. We consider here that droplets are formed due to the bubble burst process within the very thin liquid film. In view of this, we postulate that the characteristic droplet diameter, δ (presumably Sauter mean diameter) is of the same order of magnitude as the average liquid film thickness

$$\bar{l}/\delta = O(1). \quad (9)$$

Interestingly, this result agrees with the value obtained by Taylor [14] for the droplets generated due to gas blowing over shallow liquid layers, on the basis of a Kelvin–Helmholtz mechanism. Taylor assumed that droplets scale as the wavelength of the unstable wave rather than as the diameter of the ligament removed from the wave crest [15]. In addition, for shallow films it is approximated that the wavelength of the unstable wavelets scale as the average height of the wall layer [14].

From continuity requirements, the local film thickness in the absence of splashing can be given for potential flow with $u_f = u_j$ as

$$t_0 = O(d^2/r'). \tag{10a}$$

A representative value for $\bar{t}_0$ can be obtained as

$$\frac{1}{\bar{t}_0} = \frac{1}{D/2}\int_0^{D/2} \frac{1}{t_0}\,dr'.$$

Substituting for t_0 from equation (10a) in the above relation yields that

$$\bar{t}_0 = O(d/\beta). \tag{10b}$$

With droplet splashing, the average residual film thickness is reduced and becomes

$$\bar{t} \sim d(1-\alpha_c)/\beta$$

or

$$\delta \sim d(1-\alpha_c)/\beta.$$

Thus we have

$$d/\delta \sim \beta/(1-\alpha_c). \tag{11}$$

Insertion of equation (11) in equation (8) yields the relation for ϕ as

$$\phi = C_1\left(\frac{\alpha_c}{1-\alpha_c}\right)^{1/3} r^{1/3}\frac{1}{We_f^{1/3}} \tag{12}$$

where the droplet splash rate α_c and the constant C_1 are still unknown.

4.1.2. *Droplet splash rate.* An estimate for the droplet splash rate can be made based on the droplet generation due to the bubble burst process. Considering the nucleate boiling regime, we speculate that

$$\alpha \sim n$$

where n is the nucleation site density, i.e. number of bubbles generated per unit area of the heater surface.

Information on n can be obtained by analogy with pool boiling. Measurements of Katto *et al.* [1, 4] reveal that in the nucleate boiling regime, the q–ΔT characteristics of an impinging jet follows the nucleate boiling curve for ordinary pool boiling at high heat fluxes. For instance, it was mentioned in ref. [4] that the change of water depth from 100 mm to 2 mm on a heated 10 mm diameter disc surface had no effect on the boiling curve in saturated boiling at high heat fluxes greater than 5×10^5 W m^{-2}.

For a large class of factory-finished materials, a representative value of n for pool boiling is [16]

$$n \sim \Delta T^{5\text{ or }6} \sim \Delta T^{5.4}. \tag{13}$$

In pool boiling, the heat flux varies with the wall superheat for certain surfaces as

$$q \sim \Delta T^3. \tag{14}$$

Equations (13) and (14) then result in

$$\alpha \sim q^{1.8}. \tag{15}$$

This relation is in close agreement with the measurements of α by Monde and Katto [1] for water at different jet velocities, as depicted in Fig. 3. The data show that in the nucleate boiling mode increased jet velocity tends to reduce the droplet splash rate at the same wall heat flux.

Figure 3 also suggests that the droplet splash rate at the critical state α_c is nearly independent of u_j, and varies in the range of 0.8–0.9. In view of the apparent complexity of modeling α_c, we propose to determine α_c by comparing the present theory with the correlation of Katto and Shimizu [3] as given by

$$\phi = 0.188r^{0.614}\frac{1}{We_f^{1/3}}. \tag{16}$$

This relation describes data for water at 1 atm ($r = 1600$), R-113 at 1 atm ($r = 200$), and R-12 from 6–18 bar with $\beta = 5$. Comparison of equations (12) and (16) yields an expression for α_c as

$$\alpha_c = \frac{1}{1+150.5C_1^3/r^{0.842}}. \tag{17a}$$

Using an average value of $\alpha_c = 0.85$ from Monde and Katto [1] for water with $r = 1600$, the constant C_1 can be found from equation (17a) as

$$C_1 = (0.5848)^{1/3} = 0.836. \tag{17b}$$

Thus, equation (17a) reduces to

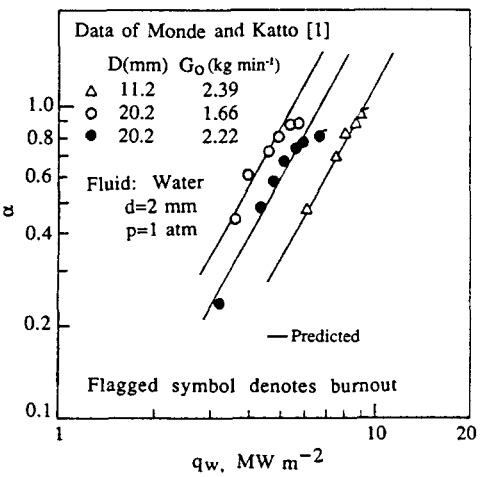

FIG. 3. Dependence of rate of splashing of droplets on wall heat flux in nucleate boiling of a saturated water jet.

$$\alpha_c = \frac{1}{1+87.98/r^{0.842}}. \quad (17c)$$

Figure 4 presents the predicted variation of α_c with density ratio. The quantity α_c is found to decrease with decreasing r. For example, for R-113 at 1 atm ($r = 200$), a value of 0.5 is predicted. For R-12 at 11.6 bar ($r = 18.2$), the value of r diminishes to 0.116. This predicted trend of α_c is in qualitative agreement with the observations of Katto and Ishii [5] that with jets of R-113 and trichloromethane there was far less spray splashed out than there was with water.

In the σ-region, the CHF varies with jet velocity ($q_c \sim u_j^{1.3}$). This regime is also called the velocity-dependent region or low velocity region. Equation (12) for the predicted CHF in the σ-controlled region should not be used for arbitrarily large values of β. Additional effects such as hydraulic jump may complicate the analysis for large values of β.

4.2. *Liquid viscosity-controlled regime (or μ-region)*

At high liquid velocities relative to the vapor, the liquid film pushes most of the vapor bubbles along the wall, and greatly diminishes the possibility of droplet formation (Fig. 2(b)). This result is evident from Fig. 4, which shows that at low values of ρ_f/ρ_g the droplet splash rate is very small.

In the limiting case of $\alpha_c \ll 1$, the mechanical energy stability criterion, equation (3), does not provide the CHF. This result suggests that the burnout is controlled by a different mechanism. In the high velocity region, we subscribe to the view of Kutateladze and Leont'ev [17] that the CHF is related to the separation of a transpired boundary layer. The problem then reduces to the estimation of the minimum vapor velocity at which the liquid flow is separated from the heated surface. In this region, the burnout is controlled by liquid viscosity, and is independent of surface tension.

A simple analysis of the CHF can now be carried out by considering the separation of the laminar boundary layer near the stagnation point. Based on the knowledge of similarity solutions for blowing near a two-dimensional stagnation point [12, 18] and accounting for the difference in densities of vapor and liquid, a criterion for the boundary layer blow-off or separation may be written as

$$\frac{\rho_g u_g}{\rho_f u_{f,x}} \sqrt{\left(\frac{\rho_f u_{f,x} r'}{\mu_f}\right)} = C_2 \quad (18)$$

where C_2 is a constant. In the absence of blowing, no separation can occur in the stagnation zone due to favorable pressure gradients.

Elimination of r' from equations (18) and (1a) results in

$$\frac{\rho_g u_g}{\rho_f u_{f,x}} \sim \sqrt{(a\nu_f)}\frac{1}{u_{f,x}}. \quad (19)$$

Using equations (7) and (19), we then obtain

$$\phi = C_2\sqrt{\left(\frac{a\nu_f}{u_j^2}\right)r}. \quad (20)$$

The dimensionless group $a\nu_f/u_j^2$ is somewhat analogous to the Reynolds number. This result shows that CHF in the high velocity and/or high pressure region is independent of surface tension and is controlled by liquid viscosity.

Measurements of the CHF in the high velocity and/or high pressure region are correlated by Katto and Shimizu [3] as

$$\phi = 1.18 r^{0.614}\frac{1}{We_f^{1/2}}. \quad (21)$$

The above result implies that the CHF is independent of jet velocity, and so this region is called the velocity-independent region.

For the purpose of comparison with equation (21), equation (20) can be cast in terms of the Weber number as

$$\phi = C_2\left(\frac{a\mu_f D}{\sigma}\right)^{1/2} r\,\frac{1}{We_f^{1/2}}. \quad (22)$$

It is possible to construct a corresponding states correlation between μ_f/σ and r in the form

$$\eta\mu_f/\sigma = f(r) \quad (23)$$

where

$$\eta = \sqrt{(\omega g_c R T_c/M)}.$$

This result is plotted in Fig. 5 which shows the vari-

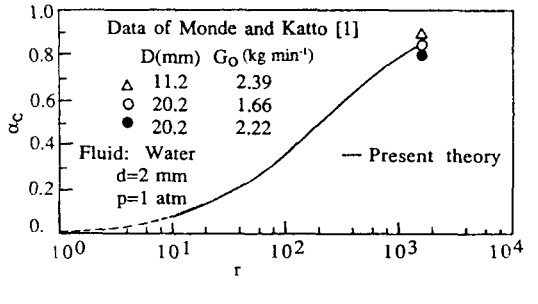

FIG. 4. Prediction of droplet splash rate at burnout.

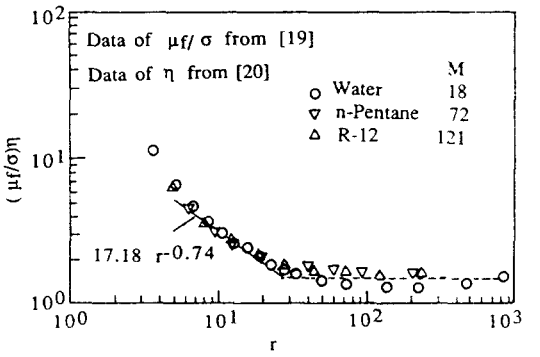

FIG. 5. Variation of μ_f/σ with density ratio.

ation of $\eta\mu_f/\sigma$ as a function of r for three different fluids—water, n-pentane and R-12. Data used in constructing Fig. 5 were taken from refs. [19, 20].

In the low pressure region ($r > 40$), μ_f/σ is nearly constant, independent of r. However, in the high pressure range ($6 < r < 20$), of greater relevance to the μ-regime being considered, μ_f/σ varies approximately according to a power law as

$$\left(\frac{\mu_f}{\sigma}\right)^{1/2} = 4.17\eta^{-1/2}r^{-0.37}, \quad 6 < r < 20. \quad (24)$$

Substituting equation (24) in equation (22), we find

$$\phi = 4.17C_2\eta^{-1/2}\sqrt{(aD)}r^{0.63}\frac{1}{We_f^{1/2}}. \quad (25)$$

Equation (25) is thus able to predict closely the observed dependence of CHF on r and We_f as correlated by equation (21) in the high pressure range ($6 < r < 20$). Denoting

$$ad/\eta \approx C_3 \quad (26a)$$

we have

$$\phi = 4.17C_2\sqrt{C_3}\sqrt{\beta}r^{0.63}\frac{1}{We_f^{1/2}}. \quad (26b)$$

A relation for the constant $C_2\sqrt{C_3}$ can be obtained by a comparison of equations (26b) and (21), ignoring the minor difference in the r-exponent

$$4.17C_2\sqrt{(C_3\beta)} = 1.18$$

$$C_2\sqrt{C_3} = \frac{1.18}{4.17\sqrt{5}} = 0.127. \quad (27)$$

Referring to equation (20), the final equation for CHF in the μ-region is written as

$$\phi = 0.127\sqrt{\left(\frac{\eta\nu_f}{du_j^2}\right)}r. \quad (28)$$

To present the results of ϕ in a single graph (Fig. 6) for both σ- and μ-regions, equations (26b) and (27) are combined to yield the following equation for ϕ in the μ-region:

$$\phi r^{-0.614} = \gamma\, We_f^{-1/2} \quad (29a)$$

where

$$\gamma = 0.127\beta^{1/2}(\eta\mu_f/\sigma)^{1/2}r^{0.386}. \quad (29b)$$

The main difficulty with the form of equation (21) is that it suppresses the effect of liquid viscosity, while it erroneously brings in the influence of surface tension. This difficulty is evident from the CHF measurements of Katto and Shimizu [3]. For instance, the data for R-12 at $p = 27.9$ bar ($r = 5$) lie consistently above those in the pressure range of 6–23.5 bar ($r = 38$ to 7) and parallel to equation (21) when $\phi/r^{0.615}$ is plotted against $1/We_f$. It is argued here that at $r \leqslant 5$, the value of μ_f/σ is higher than that given by equation (24), as indicated in Fig. 5, and therefore offers an explanation for the above discrepancy. Thus, it is clear that the proper form of correlating data in the μ-region is through equation (28) rather than equation (21).

The significance of the proposed mechanism in the high pressure and/or high velocity region and the resulting correlation equation (28) is that equation (28) can be extended for values of r smaller than those for which experimental data are available.

4.3. *Transition*

Table 1 presents the information on transition as deduced by the author from the data of Katto and Shimizu [3]. For R-12, the transition value of u_j/u_g varies weakly from 26 to 37 as the density ratio increases from 10 to 38, with a minimum value of $u_j/u_g = 26$ corresponding to $p = 17.7$ bar. No tran-

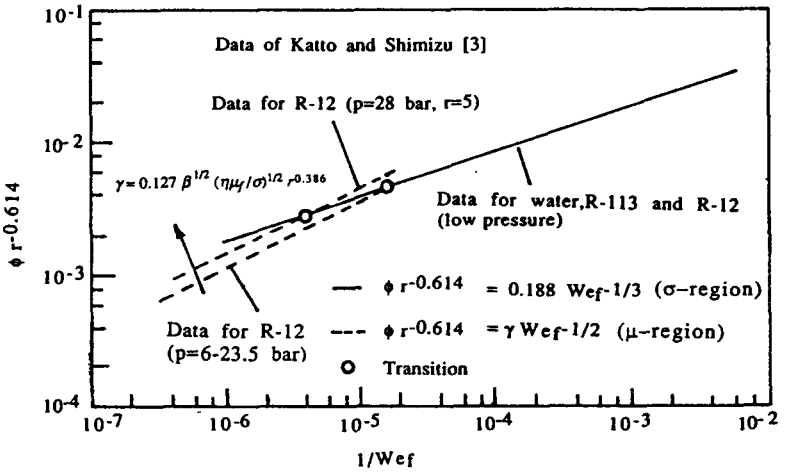

FIG. 6. Correlation of critical heat flux.

Table 1. Values of $1/\phi = u_f/u_g$ in saturated flow boiling with jet impingement from Katto and Shimizu [3]

Fluid	p (bar)	r	h_{fg} (kJ kg^{-1})	ρ_g (kg m^{-3})	$\mu_f \times 10^6$ (N s m^{-2})	$\sigma \times 10^3$ (N m^{-1})	u_j (m s^{-1})	q_c (MW m^{-2})	u_g (m s^{-1})	u_j/u_g	Region
R-12	6.0	38.5	147	29.9	224.8	8.36	2	0.9	0.21	9.5	1
							5	1.0	0.23	2.2	1
							12	1.4	0.32	37	†
							15	1.4	0.32	47	2
	11.6	18.2	127	65.4	187.0	5.9	1.1	0.85	0.10	11	1
							3	1.0	0.12	25	1
							5	1.2	0.14	36	†
							10	1.2	0.14	71	2
							17	1.2	0.14	121	2
	17.7	9.97	109	107	160.3	3.5	1.5	0.9	0.077	19	1
							2.2	1.0	0.086	26	†
							5	1.0	0.086	58	2
							17	1.0	0.086	198	2
	23.5	7.0	97.6	136	138.2	2.45	1.2	0.8	0.06	20	2
							4	0.8	0.06	67	2
							9	0.8	0.06	150	2
							18	0.8	0.06	225	2
	27.9	5.19	79.3	192	123.0	1.54	3	0.8	0.052	58	2
							7	0.75	0.052	135	2
							10	0.8	0.052	192	2
							14	0.8	0.052	269	2
Water	1.01	1603	2257	0.597	283.1	58.8	1.3	4	2.97	0.44	1
							5	6	4.4	1.1	1
							15	10	7.4	2.0	1
							50	15	11.1	4.5	1
R-113	1.01	203	146.7	7.447	507	14.56	3.7	0.6	0.55	6.7	1
							9.5	0.7	0.64	15	1
							11.9	0.8	0.73	16	1

† Transition.

sition to the μ-region is noted in the case of water ($u_j/u_g < 4.5$) and R-113 ($u_j/u_g < 16$) at $p = 1.01$ bar.

The transition between regions 1 and 2 is obtained by eliminating ϕ from equations (16) and (22)

$$0.188 r^{0.614} \frac{1}{We_f^{1/3}} = C_2 \left(\frac{a\mu_f D}{\sigma} \right)^{1/2} \frac{r}{We_f^{1/2}}.$$

This relation can be rearranged as

$$We_{f,tr}^{1/3} = \frac{C_2^2}{(0.188)^2} \left(\frac{a\mu_f D}{\sigma} \right) r^{0.772}. \quad (30)$$

With the help of equations (26a) and (27), the above equations can be recast for the transition criterion as

$$We_f^{1/3} \leqslant 0.456\beta(\eta\mu_f/\sigma) r^{0.772}: \ \sigma\text{-region}; \quad (31a)$$

$$We_f^{1/3} \geqslant 0.456\beta(\eta\mu_f/\sigma) r^{0.772}: \ \mu\text{-region}. \quad (31b)$$

Equation (31) for the transition clarifies the role of surface tension and viscosity on the CHF mechanisms with impinging jets. At high pressures involving small values of r, even small jet velocities can lead to the CHF mechanism of the μ-regime as evident from data for R-12. On the other hand, at low pressures as shown by data for water and R-113, the value of r is large, and so very large velocities are required to approach the μ-region. Furthermore, for a given jet velocity, large values of the disc-to-jet diameter ratio β can cause transition to the σ-region.

The present theory reveals that the transition Weber number $We_{f,tr}$ depends on $\mu_f\beta/\sigma$ and r, as displayed in Fig. 6. This result is in contrast with the suggestion by Katto and Shimizu [3], who proposed a constant value for $We_{f,tr}$ as

$$We_{f,tr}^{-1} = 1.64 \times 10^{-5}. \quad (32)$$

At high pressures ($r = 6$–20), $\mu_f/\sigma \sim r^{-0.774}$, so equation (30) suggests that $We_{f,tr}$ becomes constant, independent of μ_f/σ and r, and equal to that given by equation (32), as indicated by the data of R-12 ($r = 6$–20). However, at $r = 5$ and below, the value of μ_f/σ is considerably larger than the value given by equation (24), so that $We_{f,tr}$ depends on μ_f/σ and r, and exceeds that given by equation (32). Furthermore, the data of Katto and Shimizu [3] for R-113 ($r = 200$) do not seem to show transition to the μ-region, even for $We_f > We_{f,tr}$ where $We_{f,tr} = 1.64 \times 10^{-5}$ as given by equation (32). This inconsistency is easily verified by the proposed theory, equation (30), which indicates no transition for R-113 even at the maximum velocity of $u = 12$ m s^{-1}. The transition Weber number for R-113 predicted by the proposed theory is given by

$$We_{f,tr}^{-1} = 2.2 \times 10^{-8}.$$

Thus, it is clear that a single group transition criterion such as that given by equation (32) seems to be inadequate to identify the burnout mechanisms.

5. CONCLUSIONS

Based on the proposed theory for the critical heat flux in saturated forced convection over a heated disc

with an impinging jet, the following conclusions can be drawn.

(1) Two basic mechanisms of burnout were identified: a surface tension-controlled burnout and a liquid viscosity-controlled burnout.

(2) The transition Weber number, $We_{f,tr}$, between the two burnout regimes is shown to depend on two dimensionless groups r and $a\mu_f D/\sigma$.

Acknowledgements—The author is grateful to Professor John H. Lienhard of the University of Houston for valuable suggestions and discussion, and for the financial support under his DOE contract. Sherry A. Trudan of Lockheed Engineering and Sciences Company prepared the manuscript. This work was performed when the author was with the University of Houston, Department of Mechanical Engineering (1984).

REFERENCES

1. M. Monde and Y. Katto, Burnout in a high heat-flux boiling system with an impinging jet, *Int. J. Heat Mass Transfer* **21**, 295–305 (1978).
2. Y. Katto and M. Kunihiro, Study of the mechanism of burn-out in boiling system of high burn-out heat flux, *Bull. JSME* **16**, 1357–1366 (1973).
3. Y. Katto and M. Shimizu, Upper limit of CHF in the saturated forced convection boiling on a heated disk with a small impinging jet, *J. Heat Transfer* **101**, 265–269 (1979).
4. Y. Katto and M. Monde, Study of mechanisms of burnout with an impinging jet, *Proc. 5th Int. Heat Transfer Conf.*, Tokyo, pp. 245–249 (1974).
5. Y. Katto and K. Ishii, Burnout in a high heat flux boiling system with a forced supply of liquid through a plane jet, *Proc. 6th Int. Heat Transfer Conf.*, Toronto, pp. 435–440 (1978).
6. Y. Katto and S. Yokoya, Critical heat flux on a disc heater cooled by a circular jet of saturated liquid impinging at the center, *Int. J. Heat Mass Transfer* **31**, 219–227 (1988).
7. J. H. Lienhard and R. Eichhorn, On predicting boiling burnout for heaters cooled by liquid jets, *Int. J. Heat Mass Transfer* **22**, 774–776 (1979).
8. J. H. Lienhard and M. Z. Hasan, Correlation of burnout data for disk heaters cooled by liquid jets, *J. Heat Transfer* **101**, 383–384 (1979).
9. A. Sharan and J. H. Lienhard, On predicting burnout in the jet–disc configuration, *J. Heat Transfer* **107**, 398–401 (1985).
10. F. Homann, *Z. Angew. Math. Mech.* **16**, 153 (1936).
11. H. Schlichting, *Boundary Layer Theory* (6th Edn). McGraw-Hill, New York (1979).
12. F. M. White, *Viscous Fluid Flow*. McGraw-Hill, New York (1974).
13. J. E. Watson, The radial spread of a liquid jet over a horizontal plane, *J. Fluid Mech.* **20**, 481–499 (1964).
14. G. I. Taylor, Generation of ripples by wind blowing over a viscous fluid. In *The Scientific Papers of Sir Geoffrey Igram Taylor* (Edited by G. K. Batchelor), Vol. 3. Cambridge University Press, London (1963).
15. D. F. Tatterson, J. C. Dallman and T. J. Hanratty, Drop sizes in annular gas–liquid flows, *A.I.Ch.E. Jl* **23**, 68–76 (1977).
16. J. H. Lienhard, *A Heat Transfer Textbook*, p. 396. Prentice-Hall, Englewood Cliffs, New Jersey (1981).
17. S. S. Kutateladze and A. I. Leont'ev, Some applications of the asymptotic theory of the turbulent boundary layer. *Proc. 3rd Int. Heat Transfer Conf.*, Chicago (1966).
18. W. M. Kays and M. E. Crawford, *Convective Heat and Mass Transfer* (2nd Edn). McGraw-Hill, New York (1980).
19. E. U. Schlünder (Editor-in-Chief), *Heat Exchangers Design Handbook*, Part 5, *Physical Properties*. Hemisphere, Washington, DC (1983).
20. R. C. Reid, J. M. Prausmitz and T. K. Sherwood, *The Properties of Gases and Liquids* (3rd Edn). McGraw-Hill, New York (1977).

MECANISME ET PREDICTION DE L'ASSECHEMENT DANS DES EBULLITIONS FORCEES SUR DES SURFACES AVEC JET IMPACTANT

Résumé—On propose un modèle physique pour le mécanisme de l'assèchement d'ébullition en convection forcée sur des disques chauds qui sont refroidis par des jets liquides qui les frappent normalement à leur surface. On suppose que la vitesse relative entre le liquide et les bulles de vapeur dans le film pilote le mécanisme de l'assèchement. On distingue deux régions de flux thermique critique (CHF). Quand les vitesses de liquide et de vapeur sont du même ordre de grandeur, cas typique des faibles pressions, l'assèchement résulte de l'écrasement des gouttelettes et intervient la tension interfaciale. Aux faibles vitesses de vapeur par rapport au liquide, cas typique des hautes pressions, l'assèchement semble résulter de la séparation de la couche limite de liquide, et il est contrôlé par la viscosité du liquide. L'accord entre les prévisions du modèle pour le CHF avec les données disponibles dans un large domaine de rapport de densités liquide–vapeur, donne un éclairage nouveau. On suggère aussi un critère de transition entre les deux régions de CHF.

MECHANISMUS UND BERECHNUNG DES "BURNOUT" BEIM STRÖMUNGSSIEDEN AN BEHEIZTEN OBERFLÄCHEN MIT EINEM AUFPRALLENDEN STRAHL

Zusammenfassung—Ein physikalisches Modell für den Mechanismus des "Burnout" beim Sieden in gesättigter Zwangskonvektion an beheizten Scheiben wird entwickelt. Die Scheiben werden durch Flüssigkeitsstrahlen, die senkrecht auf die Oberfläche aufprallen, gekühlt. Es wird angenommen, daß die Relativgeschwindigkeit zwischen der Flüssigkeit und den Dampfblasen im Film den "Burnout"-Prozeß bestimmt. Zwei verschiedene Gebiete der kritischen Wärmestromdichte (CHF) werden festgestellt. Wenn die Geschwindigkeiten von Flüssigkeit und Dampf von gleicher Größenordung sind, dies ist typisch für kleine Drücke, wird "Burnout" von einem Versprühen von Tropfen hervorgerufen—der Vorgang ist dann oberflächenspannungsgesteuert. Wenn die Geschwindigkeit des Dampfes klein ist gegenüber der Geschwindigkeit der Flüssigkeit, dies ist typisch für hohe Drücke, scheint "Burnout" durch eine Ablösung der Flüssigkeitsgrenzschicht verursacht zu sein—der Vorgang wird in diesem Fall durch die Viskosität der Flüssigkeit gesteuert. Die Korrelation von Modellrechnungen für CHF mit den verfügbaren Daten in einem weiten Bereich des Verhältnisses von Flüssigkeits- zu Dampfdichte führt zu neuen Einblicken in die Größenordnung und die Sprühdichte der Tropfen. Schließlich wird ein Kriterium für den Übergang zwischen zwei CHF-Bereichen vorgeschlagen.

МЕХАНИЗМЫ И ОПРЕДЕЛЕНИЕ КРИЗИСА КИПЕНИЯ ПРИ ОБТЕКАНИИ НАГРЕТЫХ ПОВЕРХНОСТЕЙ НАБЕГАЮЩЕЙ СТРУЕЙ

Аннотация—Предложена физическая модель для механизма кризиса кипения насыщенной жидкости при вынужденной конвекции на нагретых дисках, охлаждаемых струями жидкости, набегающими перпендикулярно к поверхнохти. Считалось, что процесс крисиса кипения определяется относительными скоростями жидкости и пузырьков пара в пленке. Отчетливо различаются две области критических тепловых потоков (КТП). В случае, когда скорости жидкости и пара одинаковы по порядку величины, характерной для низких давлений, кризис кипения происходит за счет разбрызгивания капель и регулируется поверхностным натяжением. При более низких, по сравнению с жидкостью, скоростях пара, характерных для случаев с высоким давлением, кризис кипения вызывается отделением пограничного слоя жидкости и регулируется ее вязкостью. Согласование модели расчета КТП с имеющимися данными для широкого диапазона соотношений плотностей жидкости и пара позволило дать новое представление об установлении масштаба и скорости разбрызгивания капель. Предложен критерий перехода от одной области КТП к другой.